

Article

A New Sparse Optimal Array Design Based on Extended Nested Model for High-Resolution DOA Estimation

Shujian Wang ¹, Shiwei Ren ^{1,2} , Xiangnan Li ¹, Guiyu Wang ^{1,2}  and Weijiang Wang ^{1,2,*} ¹ School of Integrated Circuits and Electronics, Beijing Institute of Technology, Beijing 100081, China² Beijing Institute of Technology Chongqing Center for Microelectronics and Microsystems, Chongqing 401332, China

* Correspondence: wangweijiangbit@163.com

Abstract: In this paper, we propose a new strategy with increased element spacings placed on two-side subarrays and increase the physical sparse sensors array aperture. In order to ensure the continuity of difference co-array, four conditions are proposed. Based on these conditions, a new array structure named TS2-ENA is derived. Compared with other nested-like arrays with a fixed number of elements, our proposed structure possesses a higher degree of freedom, closed-form expression and outstanding performance. Simulation results show the superiority of the new configuration with the spacial smoothing MUSIC algorithm conducted.

Keywords: DOA estimation; difference co-array; nested array; degree of freedom



Citation: Wang, S.; Ren, S.; Li, X.; Wang, G.; Wang, W. A New Sparse Optimal Array Design Based on Extended Nested Model for High-Resolution DOA Estimation. *Electronics* **2022**, *11*, 3334. <https://doi.org/10.3390/electronics11203334>

Academic Editor:
Andrea De Marcellis

Received: 13 September 2022

Accepted: 14 October 2022

Published: 16 October 2022

Publisher's Note: MDPI stays neutral with regard to jurisdictional claims in published maps and institutional affiliations.



Copyright: © 2022 by the authors. Licensee MDPI, Basel, Switzerland. This article is an open access article distributed under the terms and conditions of the Creative Commons Attribution (CC BY) license (<https://creativecommons.org/licenses/by/4.0/>).

1. Introduction

As an important branch of signal processing, array signal processing has developed rapidly in recent years. Up to now, array signal processing technology has been widely used in many military and civil fields such as radar [1,2], sonar [3], communication [4], navigation [5,6], intelligent transportation [7], geological exploration and even home safety monitoring [8,9]. Direction of arrival (DOA) estimation [10] has become one of the most important topics in array research. The research focus of spatial spectrum [11] estimation is the ability of a processing system composed of spatial multi-sensor arrays to accurately estimate the spatial parameters of the spatial signal of interest, such as angle estimation accuracy, angle resolution and other spatial parameter accuracy [12,13]. The emergence of modern spectral analysis methods in the time domain has promoted the further development [14] of DOA estimation. While learning from each other, a number of new nonlinear [15] research methods have emerged, such as maximum entropy method, maximum likelihood method and linear prediction method [16]. The subspace method is a milestone in the field of super-resolution signals, including multiple signal classification method (MUSIC) [17,18] rotation invariant parameter estimation method (ESPRIT) [19,20], and the related research. All the algorithms have a great impact on DOA estimation.

Due to the continuous improvement of the super-resolution signal processing algorithm, the corresponding array structure becomes more complex step by step, and sparse array has been used [21] frequently. At this point, sparse array mainly uses a concept called difference co-array (DCA) of physical array to deal with underdetermined structures [22–25]. We can use DCA to construct a continuous virtual uniform linear array (ULA) [26,27]. The difference co-array operation can increase the physical aperture of sparse array, improve the degree of freedom (DOF) of the array, and thus perform super-resolution signal processing [28]. The design of a one-dimensional second-order sparse difference co-array is the cornerstone to design sparse arrays. Therefore, this paper mainly focuses on the design of a one-dimensional second-order difference co-array.

Sparse array was first proposed by A. Moffett in the early 1960s. The author constructed the minimum redundant array (MRA) [29] by reducing the redundancy in the

array. Due to its extremely low redundancy, the number of detectable signal sources can be more than that of physical sensors. The DOF is improved significantly. In one-dimensional second-order DCA, MRA is essentially the optimal array design, but its disadvantage lies that there is no simple closed expression for sensor locations. The array arrangement can only be obtained by computer when the total number of array elements is relatively small. Later, Pal Piya proposed nested array (NA) [30] and the concept of difference virtual co-array. Its second-order DCA can be obtained by performing differential operation on the absolute position of the actual physical sensor array. Pal Piya mathematically proved that the vectorization of the input signal is equivalent to a differential operation on the physical array [31]. The virtual DCA generated in this case makes full use of freedom, not only having non negative degrees of freedom but also negative degrees of freedom. Therefore, the available degrees of freedom of the virtual array are increased from $O(R)$ to $O(R^2)$, where R is the total number of physical array sensors. Nested array has a complete analytical construction expression for a given total number of array elements with its DCA hole-free. NA overcomes the main limitation of MRA by establishing the analytical expression of sensor position and array aperture, but its DOF capacity of NA is much lower than that of MRA. At the same time, since the use of dense ULA, the NA configuration is still susceptible to mutual coupling effects. In order to reduce the mutual coupling, in another way, and further improve the DOF at the same time, many array optimizations have been carried out on the basis of classical nested array.

Coprime nested array (CNA) [32] and improved coprime nested array (ICNA) [32] have their mutual coupling reduced. In this paper, we mainly focus on the influence of the design of the nested-like arrays (NLAs) configuration on the increase of the DOF, so the mutual coupling is not our main research direction. For DOF improvement, augmented nested array (ANA) in [33] is proposed. The ANA structure splits the dense subarray into a nested array and repositions it on both sides of the central subarray. ANA also has the hole-free DCA configuration. Next, improved nested array (INA) [34] is constructed by placing the one alone sensor outside the sparse subarray, which generates a continuous co-array and therefore further improves the DOF. However, the ANA configuration still has some problems. Since ANA's structure on both sides comes directly from the N elements of the dense subarray in the original NA, where N is the number of the dense subarray, the mutual coupling will increase, and the physical aperture of ANA arrays will not be improved very well. Recently, MISC, the maximum element spacing constraint array, is proposed [35]. This configuration generates a filled co-array which has more degrees of freedom with closed-form expression. In [36], a new idea called extended nested array (ENA) strategy was created for the consecutive co-array achievement by adding three new constraints on ANA configuration and allowing the sensors in left subarray and right subarray further than $N - 1$ but smaller than $2N$. Based on the strategy, two configurations OS-ENA and TS-ENA [36] are proposed as well, which further expand the length of co-array and enhance the DOF. However, there is still room for improvement in the DOF.

In this paper, we design a new strategy which further breaks the limitation of the distance between two subarrays in [36] and makes the sensors in left and right subarray larger than $2N$. Therefore, it can acquire a much higher number of degree of freedom for DOA estimations. It is proved that the element spacing on two-side subarrays can be extended to $2N$ distance. In order to maximize the continuity of difference co-array, we propose four conditions and improve the steps of realizing the physical array structure. Based on these conditions, a new configuration with closed-form expressions called TS2-ENA is developed, which can acquire more DOF than other NLAs, i.e., NA, ANA, MISC, OS-ENA, and TS-ENA. With the number of array elements fixed, our structure has higher degrees of freedom and better performance of target detection and azimuth estimation. Numerical results show the superiority of our designed configuration with the SS-MUSIC algorithm conducted.

The remainder of our paper is arranged as follows. The signal model and basic NLAs configuration is introduced in Section 2. Section 3 provides a detailed deduction and

description of the proposed new strategy. In Section 4, the new configuration with its associated properties and the DOF comparison with other NLAs are discussed. Section 5 provides the numerical simulation results with the spacial smoothing MUSIC algorithm conducted. Section 6 provides the conclusion for this paper.

Notations: In this paper, bold lowercase italic bold represents vector, and ordinary oblique bold represents scalar. $(\cdot)^T, (\cdot)^H$, respectively, become transpose and conjugate transpose. \odot is a Khatri–Rao product. \mathbb{A} is a collection of elements where $\{a \mid a \in \mathbb{A}\}$. \mathbf{I}_R is a $R \times R$ identity matrix. $\mathbb{E} + \mathbb{F} = \{e + f \mid e \in \mathbb{E}, f \in \mathbb{F}\}$ represents the sum set of \mathbb{E} and \mathbb{F} . $\mathbb{E} + N = \{e + N \mid e \in \mathbb{E}\}$ means that N is added to each element in \mathbb{E} . $\lfloor c \rfloor$ is the largest integer number equal to or less than c . \mathbb{N}^+ is the set of natural positive integers.

2. Base Component

2.1. Signal Model with DCA

We assume that the signal model is far-field and narrowband signals and the number is Q . Q far-field and narrowband signals impinge on a one-dimensional linear array with the number of elements R , which are located at $\mathbb{S}_s = \{p_1, p_2, \dots, p_R\}$. The received signal is:

$$\mathbf{x}(t) = \mathbf{A}\mathbf{s}(t) + \mathbf{n}(t), \tag{1}$$

here, manifold matrix $\mathbf{A} = [\mathbf{a}(\theta_1), \mathbf{a}(\theta_2), \dots, \mathbf{a}(\theta_Q)]$; $\mathbf{a}(\theta_q) = [e^{j\pi p_1 \sin(\theta_q)}, \dots, e^{j\pi p_R \sin(\theta_q)}]^T$ denotes the steering vector; $\mathbf{s}(t) = [s_1(t), s_2(t), \dots, s_Q(t)]^T$ is the signal vector; $\mathbf{n}(t)$ is the zero mean white Gaussian noise vector with variance $\sigma_n^2 \mathbf{I}_R$, where σ_n^2 is noise power. Then, the covariance matrix of $\mathbf{x}(t)$ is

$$\begin{aligned} \mathbf{R}_x &= E[\mathbf{x}(t)\mathbf{x}^H(t)] \\ &= \mathbf{A}\mathbf{R}_s\mathbf{A}^H + \sigma_n^2\mathbf{I}_R, \end{aligned} \tag{2}$$

where \mathbf{R}_s denotes the signal covariance matrix and \mathbf{R}_n is the noise energy matrix. Vectorizing \mathbf{R}_x , we have

$$\begin{aligned} \bar{\mathbf{z}} &= \text{vec}(\mathbf{R}_x) \\ &= (\mathbf{A} \odot \mathbf{A}^H)\mathbf{p} + \sigma_n^2\mathbf{1}_R, \end{aligned} \tag{3}$$

where $\mathbf{p} = [\sigma_1^2, \sigma_2^2, \dots, \sigma_Q^2]^T$; σ_q^2 is the power of the q th signal; $\mathbf{1}_R$ is the vectorization of (\mathbf{I}_R) ; $\mathbf{A} \odot \mathbf{A}^H$ is the vectorized manifold matrix. Define DCA as

$$\mathbb{D}_{\mathbb{S}} = \{p_i - p_j \mid p_i, p_j \in \mathbb{S}\}. \tag{4}$$

Select the maximum continuous segment in DCA as $\mathbb{U}_{max} = [-L_u, L_u]$ with L_u being the DOF. Then, performing spatial smoothing on the corresponding related columns or rows in $\bar{\mathbf{z}}$, we have

$$\bar{\mathbf{z}} = \bar{\mathbf{A}}\bar{\mathbf{s}} + \sigma_n^2\bar{\mathbf{1}}_R. \tag{5}$$

$\bar{\mathbf{A}}$ is the virtual manifold matrix and its dimension is $(2L_u + 1) \times Q$; $\bar{\mathbf{1}}_R = [0 \dots 0 \ 1 \ 0 \dots 0]^T$ with 1 locating at the $(L_u + 1)$ th position. After that, the SS-MUSIC method [18,37,38] can be applied on $\bar{\mathbf{z}}$ to conduct DOA estimation.

2.2. Nested-like Array Configurations

We propose an NLAs structure in this paper with the signal model based on ANA. A new design strategy is provided, which is a further extension of ENA. In this subsection, we will first introduce the structure of NLAs. Consider the nested array [26,30] configuration illustrated in Figure 1. NA has two subarrays: a sparse ULA with $M + 1$ elements locating at

$$\mathbb{S}_s = \{Npd \mid p \in [1, M + 1]\},$$

and a dense one with $N - 1$ elements at

$$\mathbb{S}_d = \{pd \mid p \in [1, N - 1]\}.$$

Here, d is the unit inter-element spacing, set as a half wavelength unit, and it will be omitted in this paper. Since a nested array has two subarrays, the total number of physical sensors $R = M + N$. Figure 1 shows a nested array with the total sensor number $R = 6$. NA's DCA is hole-free in the range $[-11, 11]$.



Figure 1. Nested array configuration with $R = 6, M = 2, N = 4$.

Based on NA configuration, ANA in [33] moves some elements of the dense subarray \mathbb{S}_d into the right side of the sparse subarray \mathbb{S}_s and forms:

$$\mathbb{S} = \mathbb{L} \cup \mathbb{M} \cup \mathbb{R}, \tag{6}$$

with

$$\begin{cases} \mathbb{L} = N - r, & r \in \mathbb{V}_1, \\ \mathbb{M} = Nr, & r \in \mathbb{V}_2, \\ \mathbb{R} = N(M + 1) + r, & r \in \mathbb{V}_3, \end{cases} \tag{7}$$

where $\mathbb{V}_2 = [1, M + 1], \mathbb{V}_1 \cup \mathbb{V}_3 = [0, N - 1], 0 \in \mathbb{V}_1$ and $0 \in \mathbb{V}_3$, here

$$\begin{cases} \mathbb{V}_1 = \{0, 1, 2, \dots, L_1\}, \\ \mathbb{V}_3 = \{0, L_1 + 1, L_1 + 2, \dots, N - 1\}, \end{cases}$$

where $L_1 < N - 1$. The elements of \mathbb{V}_1 and \mathbb{V}_2 represent the distance to the leftmost array element of \mathbb{M} . The elements of \mathbb{V}_3 represent the distance to the rightmost array element of \mathbb{M} . The number of ANA sensors R is still $N + M$. As long as \mathbb{V}_1 and \mathbb{V}_3 are reasonably distributed, a higher DOF can be achieved. Figure 2 shows an ANA configuration with the total number of sensors $R = 8$. Its DCA is consecutive in $[-21, 21]$.



Figure 2. ANA configuration with $R = 8, M = 3, N = 5$.

The ENA strategy adopts the expression of ANA in Equations (6) and (7), and it denies three new constraints on \mathbb{V}_1 and \mathbb{V}_3 to obtain a higher DOF. The TS-ENA configuration follows the ENA strategy and has the sensors located at

$$\begin{cases} \mathbb{V}_1 = \{0, e, 2e + 4 : 3e, 2e, 3e + 3\}, \\ \mathbb{V}_3 = \{0, 2e + 3, 2e + 2, e + 1, 3e + 4 : 4e\}, \end{cases}$$

where $N = 2e + 1, e \geq 5$, which further increases the length of the DCA continuous segment. Figure 3 shows a TS-ENA configuration with total number of sensors $R = 17$, and the DCA has the longest consecutive range $[-82, 82]$.

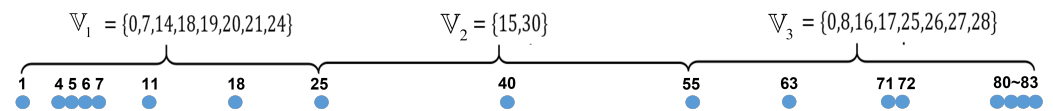


Figure 3. TS-ENA configuration with $R = 17, M = 2, N = 15$. The black numbers are the position of elements in the physical array.

3. New Strategy

In this section, we describe our new NLAs design strategy based on ENA in detail. At the same time, we have made a systematic analysis and proof of the NLAs. By modifying different constraint conditions, the mathematical model can fully and completely summarize all the NLAs that have been proposed at present, and the DOF is regarded as the only optimization target of the model.

First, we observed the structure of NA; its virtual element in DCA has the form of

$$v = N\ell_1 + \ell_2, \tag{8}$$

where $\ell_1 \in [0, M], \ell_2 \in [0, N - 1]$. Here, $\{N\ell_1 \mid \ell_1 \in [0, M]\} = \mathbb{M}$ is the middle sparse ULA with interval spacing N . As for ℓ_2 , the dense subarray in NA can be divided into two parts, \mathbb{L} and \mathbb{R} , which are distributed on both sides of the middle sparse subarray \mathbb{M} in ANA. As such, the physical aperture is increased clearly. On the basis of ANA, the ENA strategy in [36] rewrites Equation (8) into

$$v = N(\ell_1 - 1) + (N + \ell_2), \tag{9}$$

where $\ell_1 \in [1, M], \ell_2 \in [0, N - 1]$. It means that some elements in the dense subarray of \mathbb{L} and \mathbb{R} are allowed to be N further than that of ANA. Therefore, the physical aperture and DOF can be increased furthermore.

However, ENA still has its limitations on the expansion of DOF. In the extreme case, the upper limit of theoretical DOF that ENA can reach is $(2N - 1) + (2N - 2) + MN = MN + 4N - 3$, which means there is still much room for improvement. If we further increase the elements in the left and right ULAs, the largest DOF will properly be enlarged if the holes induced can be filled.

Based on this idea, we further rewrite v in DCA as

$$v = (\ell_1 - 2)N + (2N + \ell_2), \tag{10}$$

where $\ell_1 \in [2, M], \ell_2 \in [0, N - 1]$. As such, the elements in the dense subarray \mathbb{L} and \mathbb{R} can locate $2N$ further than ANA. The physical aperture will break the limit of the ENA strategy as well. Meanwhile, holes may be generated for the sparser distribution of two-side subarrays. Taking NA as an example, the section $[0, N - 1]$ is originally continuous in DCA. When ANA divides it into left and right ULAs of the designed subarray, one condition has to be added to ensure its continuity. On this basis, ENA adds N to some of its elements, which requires more strict conditions to ensure the continuity of the range $[0, N - 1]$ in DCA. Similarly, our new strategy should pay more attention to the possible holes generated by sparse location, especially in the range $[0, 2N - 1]$ for our strategy. To ensure the continuity of DCA, four necessary conditions are proposed as below.

Theorem 1. Assume a new array configuration with Equations (6) and (7). In case \mathbb{V}_1 and \mathbb{V}_3 satisfy the following four conditions:

- (1) $\mathbb{D}_{\mathbb{V}_1} \cup \mathbb{D}_{\mathbb{V}_3} \cup [N + \mathbb{F}^-(\mathbb{V}_1)] \cup [N + \mathbb{F}^-(\mathbb{V}_3)] \supseteq [0, 2N - 1]$;
- (2) $\mathcal{R}[\mathbb{V}_1 \cup \mathbb{V}_3]_N = [0, N - 1]$;
- (3) $\mathbb{V}_1 \oplus \mathbb{V}_3 \supseteq [\mathbb{F}^-(\mathbb{V}_1) \cup \mathbb{F}^-(\mathbb{V}_3)] + N$;
- (4) $\mathbb{V}_1 \oplus \mathbb{V}_3 \supseteq [2N, T]$, where T is a positive integer bigger than $2N$.

The positive DCA \mathbb{D}_S will be continuous in the range $[0, MN + T]$. Here, $\mathbb{D}_A = \{p_1 - p_2 \mid p_1, p_2 \in \mathbb{A}, p_1 \geq p_2\}$; $\mathcal{R}[\mathbb{A}]_b$ is the remainder of $\{a/b \mid a \in \mathbb{A}\}$; $\mathbb{F}^-(\mathbb{A}) = \{a \mid a < N, a \in \mathbb{A}\}$. Especially, we set $\mathbb{F}(\mathbb{H}) = \{h \mid N \leq h < 2N, h \in \mathbb{H}\}$, $\mathbb{F}^+(\mathbb{H}) = \{h \mid 2N \leq h < 3N, h \in \mathbb{H}\}$.

Proof of Theorem 1. We divide the whole positive DCA into three parts, $v \in [0, 2N - 1]$, $v \in [2N, MN + 2N - 1]$ and $v \in [MN + 2N, T]$, in which all the elements v can be differentially expressed by the positions of the actual physical array elements, thus completing the proof of our new strategy. First of all,

(a) If the DCA virtual element $v \in [0, 2N - 1]$, there are three situations as follows:

- (1) If $v \in \mathbb{D}_{V_1} \cup \mathbb{D}_{V_3}$, v is the self-difference element, it is easy to see that $v \in [0, 2N - 1] \subseteq \mathbb{D}_S$;
- (2) If $v \in [\mathbb{F}^-(V_1) + N]$, then we can rewrite v as:

$$v = 2N - (N - \mathbb{F}^-(V_1)), \tag{11}$$

when $M \geq 2$, where $2N \in \mathbb{M}$, $(N - \mathbb{F}^-(V_1)) \in \mathbb{L}$; v can be produced by the difference between the sensors of the middle part and the left part. When $M = 1$, $2N \in \mathbb{R}$, $(N - \mathbb{F}^-(V_1)) \in \mathbb{L}$, v can be produced by the difference between the elements of the right part and the left part.

- (3) If $v \in [\mathbb{F}^-(V_3) + N]$, then we can rewrite v as:

$$v = (M + 1)N + (\mathbb{F}^-(V_3)) - MN, \tag{12}$$

where $(M + 1)N + (\mathbb{F}^-(V_3)) \in \mathbb{R}$, $MN \in \mathbb{M}$. v can be produced by the difference between the elements of the middle part and the right part.

Therefore, in this part $[0, 2N - 1]$, v can be found in DCA, and the lag $[0, 2N - 1]$ in DCA is hole-free.

- (b) If the DCA virtual element $v \in [2N, MN + 2N - 1]$, let $V'_1 = \mathbb{F}^-(V_1 \cup V_3)$, $V'_3 = \mathbb{F}(V_1 \cup V_3)$, $V''_3 = \mathbb{F}^+(V_1 \cup V_3)$. When $v \in [2N, MN + N - 1]$, we can rewrite v as

$$v = \ell_1 N + \ell_2, \ell_1 \in [2, M], \ell_2 \in [0, N - 1]. \tag{13}$$

Then, $\ell_2 \in V'_1 \cup \mathcal{R}[V'_3]_N \cup \mathcal{R}[V''_3]_N$;

- (1) If $\ell_2 \in V'_1$, then we can let v become:

$$v = N(\ell_1 + 1) - (N - \ell_2), \tag{14}$$

where $\ell_1 \in [2, M]$, $\ell_2 \in V'_1$. Obviously, for $\ell_1 \neq M$, $N(\ell_1 + 1) \in \mathbb{M}$, while for $\ell_1 = M$, $N(\ell_1 + 1) \in \mathbb{R}$. In another way, $N - \ell_2 \in \mathbb{L}$. So, v can be produced by the difference between the sensors of the middle or right part and the left part.

- (2) If $\ell_2 \in \mathcal{R}[V'_3]_N$, then we rewrite the form of v as

$$\begin{aligned} v &= N(\ell_1 - 1) + (N + \ell_2) \\ &= \underbrace{(N + NM + \ell_2)}_{\in \mathbb{R}} - \underbrace{N(M + 1 - \ell_1)}_{\in \mathbb{M}}. \end{aligned} \tag{15}$$

Obviously, it is the difference element between the right and middle subarrays.

- (3) If $\ell_2 \in \mathcal{R}[V''_3]_N$, then v should be rewritten to

$$\begin{aligned} v &= N(\ell_1 - 2) + (2N + \ell_2) \\ &= \underbrace{(2N + MN + \ell_2)}_{\in \mathbb{R}} - \underbrace{N(M + 2 - \ell_1)}_{\in \mathbb{M}}. \end{aligned} \tag{16}$$

It is also the difference element between the right and middle subarrays.

When $v \in [MN + N, MN + 2N - 1]$, v can be as:

$$v = MN + \ell, \ell \in [N, 2N - 1]. \tag{17}$$

Then, $\ell \in [\mathbb{V}'_1 + N] \cup \mathbb{V}'_3 \cup [\mathbb{V}''_3 - N]$:

- (4) If $\ell \in [\mathbb{V}'_1 + N]$, according to condition (3), $\mathbb{V}_1 \oplus \mathbb{V}_3 \supseteq [\mathbb{V}'_1 + N]$, we have $\ell \in \mathbb{V}_1 \oplus \mathbb{V}_3$, and v can be as

$$\begin{aligned} v &= NM + \ell_1 + \ell_2 \\ &= \underbrace{(NM + N + \ell_2)}_{\in \mathbb{R}} - \underbrace{N - \ell_1}_{\in \mathbb{L}}, \end{aligned} \tag{18}$$

where $\ell_1 \in \mathbb{V}_1, \ell_2 \in \mathbb{V}_3$. It is the difference element between the right and left subarrays.

- (5) If $\ell \in \mathbb{V}'_3$, then v can be as

$$\begin{aligned} v &= NM + \ell \\ &= \underbrace{(NM + N + \ell)}_{\in \mathbb{R}} - \underbrace{N}_{\in \mathbb{M}}. \end{aligned} \tag{19}$$

It is the difference element between the right and middle subarrays.

- (6) If $\ell \in [\mathbb{V}''_3 - N]$, then v can be rewritten as:

$$v = N(M - 1) + \ell = N(M + 1) + \ell + N - 2N, \tag{20}$$

when $M = 1, 2N \in \mathbb{R}$; while for $M \geq 2, 2N \in \mathbb{M}$. In another way, $N(M + 1) + N + \ell \in \mathbb{R}$. So, v can be produced by the difference among these three subarrays.

Therefore, in this lag $[2N, MN + 2N - 1]$, v can be found in DCA, and the lag $[0, 2N - 1]$ in DCA is hole-free.

- (c) If the DCA virtual element $v \in [MN + 2N, T]$, then v can be as $v = MN + \ell_2$, where $\ell_2 \in [2N, T]$. According to condition (4), $\mathbb{V}_1 \oplus \mathbb{V}_3 \supseteq [2N, T]$, we have $\ell_2 \in \mathbb{V}_1 \oplus \mathbb{V}_3$. In this way, v can be as

$$\begin{aligned} v &= \ell_{21} + \ell_{22} + NM \\ &= \underbrace{(NM + N + \ell_{22})}_{\in \mathbb{R}} - \underbrace{N - \ell_{21}}_{\in \mathbb{L}}, \end{aligned} \tag{21}$$

where $\ell_{21} \in \mathbb{V}_1, \ell_{22} \in \mathbb{V}_3$. This is the difference result between the \mathbb{R} and \mathbb{L} subarray. Therefore, v in the range of $[MN + 2N, MN + T]$ can be found in DCA.

In the end, any element in DCA can be produced by two mutual differences or self differences in these three subarrays, and the DCA is consecutive in $[0, MN + T]$. □

Theorem 1 further releases the constraints on \mathbb{V}_1 and \mathbb{V}_3 compared with the ENAs. As such, the elements on both sides will locate N sparser than TS-ENA. In this case, the two largest elements in \mathbb{L} and \mathbb{R} will become $3N - 1$ and $3N - 2$. With the elements of $\mathbb{V}_1, \mathbb{V}_3$ properly chosen, many new structures can be constructed. In the next subsection, we will introduce one configuration that satisfies the conditions in Theorem 1 and has a higher DOF than the existing nested-like structures.

Remark 1. Generally, the upper limit of theoretical DOF that Theorem 1 can reach will be $MN + (3N - 1) + (3N - 2) = MN + 6N - 3$. Theorem 1 relocates the elements in \mathbb{V}_1 and \mathbb{V}_3 so that the two largest elements become $(N - 1) + 2N$ and $(N - 2) + 2N$, i.e., $3N - 1$ and $3N - 2$. In the upper limit situation, $3N - 1$ and $3N - 2$ are assigned to the left subarray and right subarray,

respectively. With DCA hole-free, its upper limit will reach $MN + 6N - 3$. Compared with the upper limit $MN + 4N - 3$ of ENA, the proposed new strategy owns more complex constraints for higher degrees of freedom.

4. Proposed Array Configuration and Properties

In this section, we devise a new configuration based on the new strategy, discuss the corresponding properties and compare it with other NLAs.

4.1. Proposed New Configuration

Definition 1. For $N = 4L + 3, L > 6$ and $M \geq 1$, a twice-sparse double extended nested array, named TS2-ENA, can be expressed by Equations (6) and (7) with

$$\begin{cases} \mathbb{V}_1 = \{0, 2L + 1, 4L + 2, 6L + 3, 8L + 4, \\ \quad 8L + 9 : 10L + 5, 12L + 2 : 12L + 5\}, \\ \mathbb{V}_3 = \{0, 2L + 2, 4L + 4, 6L + 6, 8L + 8, \\ \quad 10L + 10 : 12L + 1, 12L + 6\}. \end{cases} \tag{22}$$

The TS2-ENA configuration has the same three-stage structure as ANA. The difference is the element spacing is mainly expanded by the sparse subarray in the middle. The left and right side subarrays further enlarge the spacing of some elements, thus increasing the aperture of physical array. Due to the constraints in Theorem 1, the DCA of our new configuration maintains continuity from 0 to $MN + T$. Therefore, the DOF is greatly improved. Figure 4 shows the array elements distribution of our new configuration. For easy understanding, we set the position coordinate of the first array element as 1.

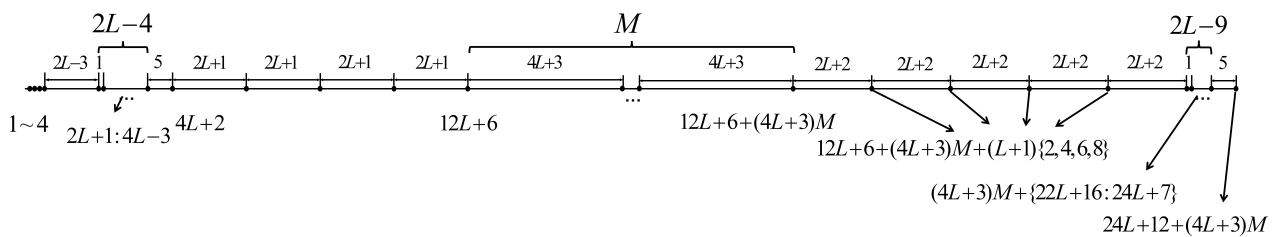


Figure 4. TS2-ENA with visual distribution configuration.

Property 1. The DCA of TS2-ENA keeps continuous in $[0, L_u]$. $L_u = MN + 6N - 12$, which is the one-side positive DOF.

Proof of Property 1. According to proposed structure and natural number pair $N = 4L + 3, L > 6$ and $M \geq 1$, we have

- (a) $\mathbb{D}_{\mathbb{V}_1} = \{1 : 2L - 4, 1 : 3, 2L + 1, 4L + 2, 6L + 3, 6L + 8 : 8L + 4, 10L + 1 : 10L + 4, 4L + 7 : 6L + 3, 8L : 8L + 3, 2L + 6 : 4L + 2, 6L - 1 : 6L + 2, 5 : 2L + 1, 4L - 2 : 4L + 1, 2L - 3 : 4L - 4\} \cup \mathbb{V}_1,$
 $\mathbb{D}_{\mathbb{V}_3} = \{1 : 2L - 9, 2L + 2, 4L + 4, 6L + 6, 8L + 8 : 10L - 1, 10L + 4, 6L + 6 : 8L - 3, 8L + 2, 4L + 4 : 6L - 5, 6L, 2L + 2 : 4L - 7, 4L - 2, 5 : 2L - 4\} \cup \mathbb{V}_3,$
 $\mathbb{D}_{\mathbb{V}_1} \cup \mathbb{D}_{\mathbb{V}_3} = \{0 : 6L + 3, 6L + 6 : 8L + 4\},$
 $[N + \mathbb{F}^-(\mathbb{V}_1)] = \{4L + 3, 6L + 4, 8L + 5\},$
 $[N + \mathbb{F}^-(\mathbb{V}_3)] = \{4L + 3, 6L + 5\}.$
 Therefore, $\mathbb{D}_{\mathbb{V}_1} \cup \mathbb{D}_{\mathbb{V}_3} \cup [N + \mathbb{F}^-(\mathbb{V}_1)] \cup [N + \mathbb{F}^-(\mathbb{V}_3)] \supseteq [0, 8L + 5] = [0, 2N - 1]$. The first condition of Theorem 1 is perfect coincidence
- (b) On the second condition of Theorem 1, we have

$$\begin{aligned} \mathcal{R}[\mathbb{V}_1 \cup \mathbb{V}_3]_N &= \{0, 2L + 1, 4L + 2, 2L, 4L + 1, \\ &3 : 2L - 1, 4L - 4 : 4L - 1\} \cup \{0, 2L + 2, \\ &1, 2L + 3, 2, 2L + 4 : 4L - 5, 4L\} \\ &= [0, 4L + 2] = [0, N - 1]. \end{aligned}$$

Therefore, we conclude that $\mathcal{R}[\mathbb{V}_1 \cup \mathbb{V}_3]_N = [0, N - 1]$.

$$\begin{aligned} \text{(c)} \quad &[\mathbb{F}^-(\mathbb{V}_1) \cup \mathbb{F}^-(\mathbb{V}_3)] + N = \{4L + 3, 6L + 4, 6L + 5, 8L + 5\}; \\ &\mathbb{V}_1 \oplus \mathbb{V}_3 \supseteq \{2L + 1, 4L + 2, 6L + 3, 8L + 4\} \cup \\ &\{2L + 2, 4L + 4, 6L + 6\} \cup \\ &\underbrace{\{4L + 3, 6L + 4, 6L + 5, 8L + 5\}}_{\mathbb{A}_1} \cup \underbrace{\{8L + 6 : 24L + 6\}}_{\mathbb{A}_2}, \end{aligned}$$

where $\mathbb{A}_1 = [\mathbb{F}^-(\mathbb{V}_1) \cup \mathbb{F}^-(\mathbb{V}_3)] + N$; $\mathbb{A}_2 = [2N, 6N - 12] = [2N, T]$. As a result, it can be deduced that conditions (3) and (4) can be satisfied.

Finally, from the above simple proof, the TS2-ENA satisfies these four conditions in Theorem 1. It is clearly that the DCA is consecutive in $[0, MN + 6N - 12]$. Its DOF is $L_u = MN + 6N - 12$. □

Property 2. For a fixed total positive integer number R , the optimal ratio of N , M and the upper limit form of a one-side degree of freedom are displayed in Table 1.

Table 1. Optimal parameters of array.

	Optimal N	Maximum-DOF
Values	$4\lfloor \frac{R+3}{8} \rfloor + 3$	$O((\frac{R}{2})^2 + 3R)$

It can be seen from Property 2 that to maximize the DOF, we should have to set a reasonable value of N and then determine the value of M by $N + M = R$. This problem actually can be translated into an optimization problem:

$$\begin{aligned} \max \quad &MN + 6N - 12 \\ \text{s.t.} \quad &M + N = R \\ &N = 4L + 3 \\ &L > 6 \\ &M, L \in \mathbb{N}^+ \end{aligned}$$

By solving this optimization problem, we can obtain the N and DOF of the optimal solution, which are shown in Table 1.

Figure 5 shows an array configuration of TS2-ENA with $N = 31, M = 1$. As shown, some sensors are set $2N + \ell (\ell \in [0, N - 1])$ away from \mathbb{M} , which includes $\{1 \dots 4, 15 \dots 25\}$ in \mathbb{L} and $\{185, 201 \dots 206, 211\}$ in \mathbb{R} . Meanwhile, the elements with $N + \ell$ away from \mathbb{M} are $\{30, 45\}$ in \mathbb{L} and $\{153, 169\}$ in \mathbb{R} . In TS2-ENA’s virtual DCA, it is hole-free in $[0, 205]$ and has one hole in 206. Due to the increase of actual sensors aperture and continuous lags in DCA, the DOF can be improved significantly.

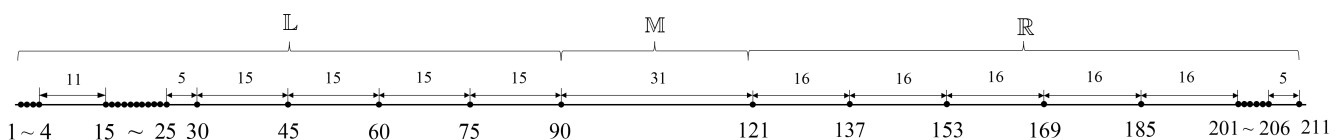


Figure 5. An example of TS2-ENA with $N = 31, M = 1, R = 32$.

4.2. DOF Ratio and Comparison

In this section, we mainly discuss the property of DOF. In practical application, the purpose of performing a second-order differential operation on a physical array is to expand its virtual aperture, i.e., a one-side positive DOF L_u . It is also the most intuitive evaluation index for the design of a one-dimensional sparse array. Therefore, the first batch

of experiments is to compare and analyze the DOF of each nested-like array structure with the same number of array elements.

Firstly, we comprehensively consider all recently proposed NLAs and list their optimal configuration parameters and other properties in Table 2. The new structure has the highest degree of freedom compared with other configurations. With the fixed number R , the DOF of TS2-ENA can reach $O((R/2)^2 + 3R)$, which are followed by TS-ENA, OS-ENA, and MISC. ANAI-2, CNA and NA are the three with relatively smaller degrees of freedom. However, TS2-ENA requires a higher total number of elements for the configuration. Meanwhile, its optimal parameters for maximizing DOF can only be set when the total number of elements is greater than or equal to 32. In the whole DCA, there is a hole at $MN + 6N - 11$, but its longest continuous segment is still larger than that of the DCA of other structures.

Table 2. DOF comparison of nested-like arrays .

Configuration	DOF	Optimal N	Max DOF
NA [30]	$MN + N - 1$	$\lfloor \frac{R+1}{2} \rfloor$	$O((R/2)^2 + 0.5R)$
CNA [32]	$\lceil \frac{R+1}{2} \rceil \lfloor \frac{R+1}{2} \rfloor - 1$	$\lfloor \frac{R+1}{2} \rfloor$	$O((R/2)^2 + 0.5R)$
ANAI [33]	$MN + 2N - 4$	$\lfloor \frac{R}{2} \rfloor + 1$	$O((R/2)^2 + R)$
MISC [35]	$MN + 3N - 7$	$2\lfloor \frac{R}{4} \rfloor + 2$	$O((R/2)^2 + 1.5R)$
OS-ENA [36]	$MN + 3N - 5$	$2\lfloor \frac{R}{4} \rfloor + 2$	$O((R/2)^2 + 1.5R)$
TS-ENA [36]	$MN + 3.5N - 3.5$	$2\lfloor \frac{R+3}{4} \rfloor + 1$	$O((R/2)^2 + 1.75R)$
TS2-ENA	$MN + 6N - 12$	$4\lfloor \frac{R+3}{8} \rfloor + 3$	$O((R/2)^2 + 3R)$

Then, we define a new DOF ratio as:

$$\delta = R^2/2\lambda, \tag{23}$$

where λ is the physical aperture of the sparse array. The smaller the DOF ratio, the higher the DOF and the better the effect with R fixed. Figure 6 shows the DOF rate δ of five configurations of NA, ANA, OS-ENA, TS-ENA and our proposed TS2-ENA nested-like arrays. The variation range of R is from 50 to 100. We select the optimal configurations for comparison of all structures. From this picture, we can understand that the DOA estimation capability of the proposed configuration TS2-ENA is the best.

Figure 7 illustrates the trend of the physical aperture of the above five NLAs with the growth of the number of physical sensors. We can see that the physical aperture of NLAs is about the order of $O(R^2)$, while the array physical aperture of our new structure is the biggest with the same number of array sensors. This is because our expansion of the subarray on both sides is superior to other NLAs in the order of $O(R)$, which makes the physical aperture significantly larger. As can be seen, our new structure has extraordinary advantages in terms of physical aperture.

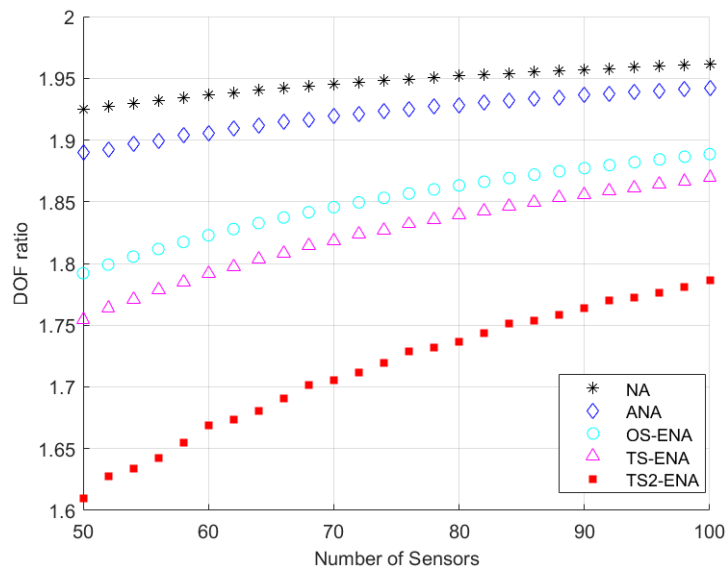


Figure 6. DOF ratio vs. number of sensors.

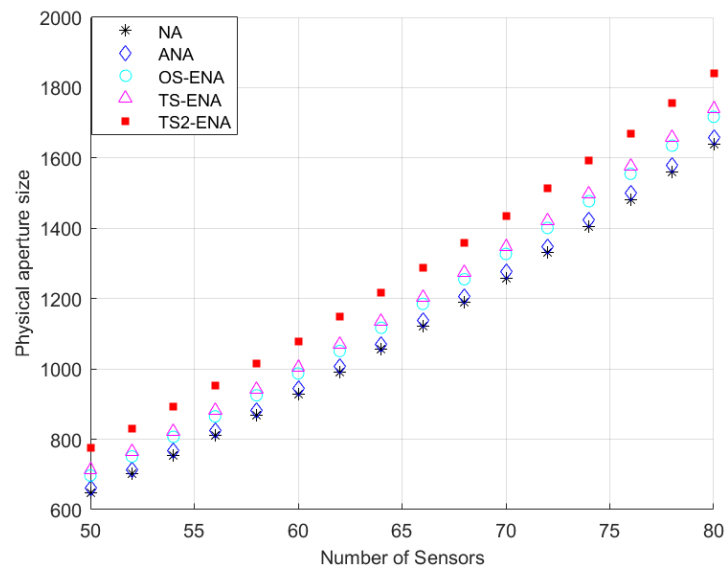


Figure 7. Physical aperture vs. number of sensors

5. Numerical Experiment

In this section, several simulations are conducted, including DOA estimation spectra and accuracy error analysis for performance comparisons.

In order to compare the performance of these configurations more intuitively, it is necessary to further compare and observe the DOA estimation results of each nested-like array. The first experimental simulation is to show the DOA estimation results of six NLAs: NA, ANA, MISC, OS-ENA, TS-ENA and TS2-ENA. Consider that $D = 150$ uncorrelated sources impinge on these configurations with $R = 50$, which is uniformly distributed between -60° and 60° . These formations all use the best parameters. We set the signal to noise ratio (SNR) as 5 dB, and then, we set snapshot K as 1000. The SS-MUSIC is used for DOA estimation based on DCA.

As shown in Figure 8, NA, ANA, MISC, OS-ENA and TS-ENA have some sources undetected when the number of sources is large, which is caused by the insufficient capacity of the DOF. Since the DOF of our structure is the highest, the number of detected sources is also the largest. The search of 150 spectral peaks can be well realized.

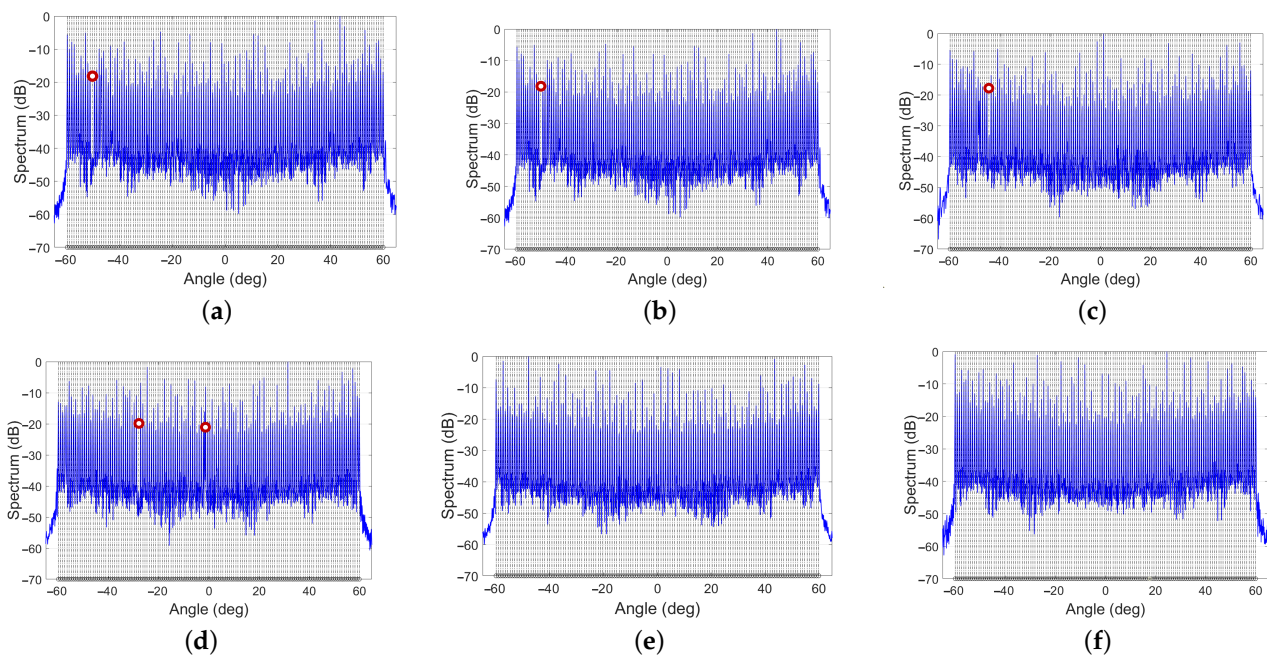


Figure 8. Simulation diagram of DOA estimation for six sparse arrays. The red circle indicates that there is a wrong spectral peak at this position. (a) NA. (b) ANA. (c) MISC. (d) OS-ENA. (e) TS-ENA. (f) TS2-ENA.

In the second experiments, we compare and estimate the DOA estimation accuracy of six NLAs configurations through the root-mean-square error (RMSE):

$$RMSE = \sqrt{\frac{1}{300Q} \sum_{i=1}^{300} \sum_{q=1}^Q (\hat{\theta}_q(i) - \theta_q)^2}, \quad (24)$$

where $\hat{\theta}_q(i)$ is the estimation of θ_q for the i^{th} trial with 300 Monte Carlo trials. The number of sources to be detected is set as $D = 200$ in the three experiments.

Figure 9 shows the SNR versus number of sensors. The RMSE results is different from -10 to 15 dB. In this part, K is set as 1000. It can be seen from the result that as the SNR increases, the influence of noise will decrease, resulting in the RMSE of each array being smaller and the accuracy of estimation improved. At about 10 dB, CNA further reduces its RMSE due to the inhibition of mutual coupling. Meanwhile, other structures basically depend on the DOF with RMSE gradually decreasing. The RMSE of our new structure TS2-ENA is consistently the smallest, which indicates that its estimation accuracy is better than other array models.

In Figure 10, we give the the parameters with $SNR = 5$ dB and set snapshots from 1 to 3000. In this picture, we can conclude that with the continuous expansion of snapshots and sampling data, this RMSE will gradually decrease and then tend to be stable. When K is small, the error of nested-like arrays is obviously large. When K is larger than 1500, the RMSE of each structure will decrease significantly. Especially, the RMSE of TS-ENA and CNA will decrease significantly. Since CNA is optimized for mutual coupling and TS-ENA has the highest DOF, they both have good simulation performance. The RMSE of our proposed configuration is the smallest all the time.

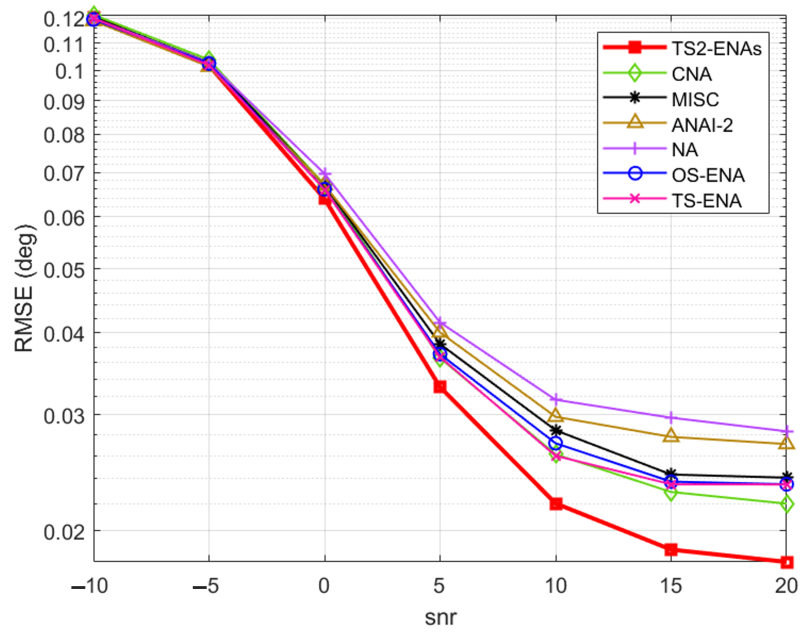


Figure 9. RMSE vs. snr.

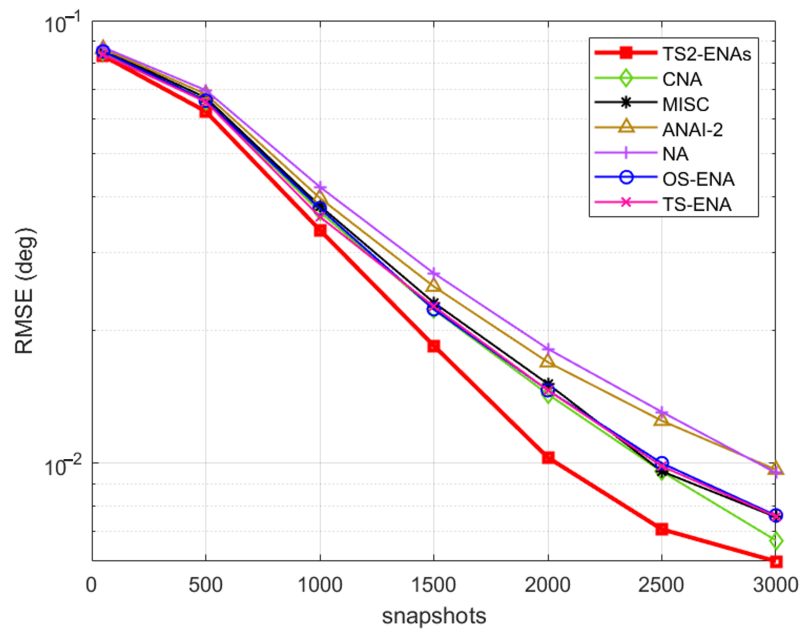


Figure 10. RMSE vs. snapshots.

Figure 11 shows that as the number of measured sensors increases, the minimum mean square error increases gradually. This experiment illustrates the RMSE versus number of sources from 100 to 200 with $K = 1000$, $SNR = 5$ dB. Since the DOF of each structure is different, the RMSE will also increase when the number of detected sources is large. With the increase of number of sources, the array with the smallest influence of error rate is TS2-ENA, which is followed by CNA, MISC, TS-ENA, OS-ENA and ANA.

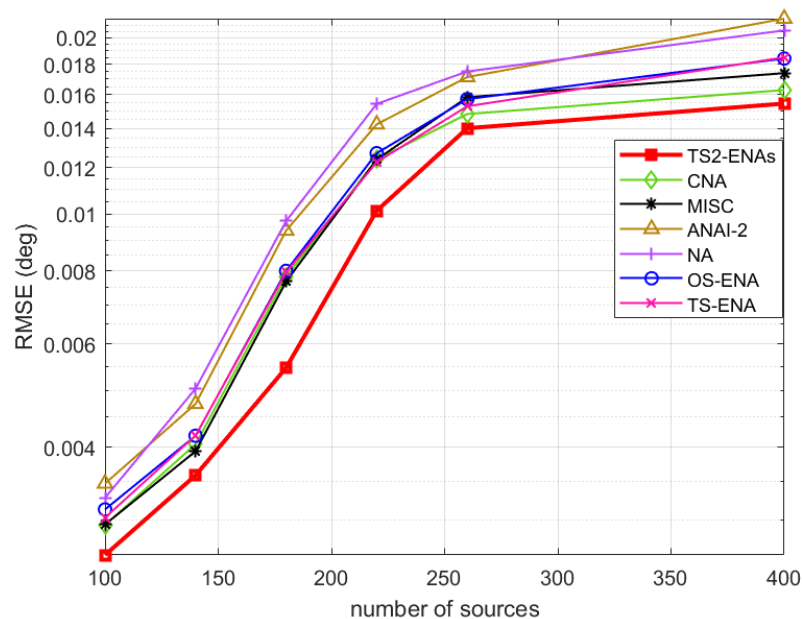


Figure 11. RMSE vs. number of sources.

6. Conclusions

To obtain the DOF enhancement, a new nested array design strategy is proposed and finished in our paper. To maximize the continuity of DCA, we propose four conditions. Based on these conditions, a new configuration referred to as TS2-ENA sparse array with closed-form expression is developed. With the number of array elements fixed, our structure has higher degrees of freedom and better performance in target detection and azimuth estimation. The simulation results show the advantages of our new configuration. It should be mentioned that there is still room for improvement for \mathbb{V}_1 and \mathbb{V}_3 . In addition, in the case of bilateral multiple expansion, the DOF of the general solution does not reach the theoretical upper limit of this paper, which means that the general solution may not be the optimal solution. These will be studied in the future.

Author Contributions: S.W. proposed the original idea of the full text. S.R. and G.W. designed and implemented the simulation experiments. X.L. and W.W. analyzed the results. S.W. and W.W. drafted the article. All authors have read and agreed to the published version of the manuscript.

Funding: This work was supported by the National Natural Science Foundation of China under Grant No. 61801024 and the Chongqing Natural Science Foundation under Grant No. cstc2021jcyj-msxmX1096. (Corresponding author: Weijiang Wang). The authors are with the school of Integrated Circuits and Electronics, Beijing Institute of Technology, Beijing 100081, China. Shiwei Ren, Guiyu Wang and Weijiang Wang are also with BIT Chongqing Institute of Microelectronics and Microsystems, Chongqing 401332, China. (email: renshiwei@bit.edu.cn).

Conflicts of Interest: The authors declare no conflict of interest.

References

- Zhang, W.; He, Z.S. Comments on “waveform optimization for transmit beamforming with mimo radar antenna array”. *IEEE Trans. Antennas Propag.* **2018**, *66*, 6463. [CrossRef]
- Herd, J.S.; Conway, M. The evolution to modern phased array architectures. *Proc. IEEE* **2016**, *104*, 519–529. [CrossRef]
- Ganti, A. Calibration and direction of arrival performance of sonar arrays composed of multiple sub-arrays. In Proceedings of the MTS/IEEE Charleston OCEANS Conference, Charleston, SC, USA, 22–25 October 2018.
- Huang, W.; Huang, Y.; Zeng, Y.; Yang, L. Wideband millimeter wave communication with lens antenna array: Joint beamforming and antenna selection with group sparse optimization. *IEEE Trans. Wireless Commun.* **2018**, *10*, 6575–6589. [CrossRef]
- Albrektsen, S.M.; Bryne, T.H.; Johansen, T.A. Phased array radio system aided inertial navigation for unmanned aerial vehicles. In Proceedings of the 2018 IEEE Aerospace Conference, Big Sky, MT, USA, 3–10 March 2018.

6. Guo, Q.; Deng, W.H.; Bebek, O.; Cavusoglu, M.C.; Mastrangelo, C.H.; Young, D.J. Personal inertial navigation system assisted by mems ground reaction sensor array and interface ASIC for GPS-denied environment. *IEEE J. Solid-State Circuits* **2018**, *53*, 3039–3049. [[CrossRef](#)]
7. Dimitrov, K.; Dzhezhev, K.; Mitsev, T. Enhancing smart-home environments using infrared arrays. In Proceedings of the National Conference with International Participation, Sofia, Bulgaria, 17–18 May 2018.
8. Liang, Q.; Mpanda, R.S.; Xin, W.; Shi, J.; Xu, L. A printed dipole array antenna for non-contact monitoring system. In Proceedings of the 2018 Cross Strait Quad-Regional Radio Science and Wireless Technology Conference (CSQRWC), Xuzhou, China, 21–24 July 2018.
9. Schafer, S.; Diewald, A.R.; Schmiech, D.; Muller, S. One-dimensional patch array for microwave-based vital sign monitoring of elderly people. In Proceedings of the 2018 19th International Radar Symposium (IRS), Bonn, Germany, 20–22 June 2018.
10. Liu, J.; Zhang, Y.; Wang, W.; Lu, Y. Generalized design method for the difference co-array of the sum co-array. In Proceedings of the IEEE International Conference on Digital Signal Processing, Beijing, China, 16–18 October 2016.
11. Pillai, S.U.; Haber, F. Statistical analysis of a high resolution spatial spectrum estimator utilizing an augmented covariance matrix. *IEEE Trans. Acoust. Speech Signal Process.* **1987**, *35*, 1517–1523. [[CrossRef](#)]
12. Ma, W.K.; Hsieh, T.H.; Chi, C.Y. DoA estimation of quasi-stationary signals via Khatri-Rao subspace. In Proceedings of the IEEE International Conference on Acoustics, Taipei, Taiwan, 19–24 April 2009.
13. Ma, W.K.; Hsieh, T.H.; Chi, C.Y. DoA estimation of quasi-stationary signals with less sensors than sources and unknown spatial noise covariance: A Khatri-Rao subspace approach. *IEEE Trans. Signal Process.* **2010**, *58*, 2168–2180. [[CrossRef](#)]
14. Pillai, S.U.; Bar-Ness, Y.; Haber, F. A new approach to array geometry for improved spatial spectrum estimation. *Proc. IEEE* **1985**, *73*, 1522–1524. [[CrossRef](#)]
15. Chevalier, P.; Ferreol, A. On the virtual array concept for the fourth-order direction finding problem. *IEEE Trans. Signal Process.* **1999**, *47*, 2592–2595. [[CrossRef](#)]
16. Abramovich, I.Y.; Gray, A.D.; Gorokhov, Y.A.; Spencer, K.N. Positive-definite Toeplitz completion in DoA estimation for nonuniform linear antenna arrays. I. Fully augmentable arrays. *IEEE Trans. Signal Process.* **1998**, *46*, 2458–2471. [[CrossRef](#)]
17. Krim, H. Two decades of array signal processing research. *IEEE Signal Process. Mag.* **1994**, *13*, 67–94. [[CrossRef](#)]
18. Schmidt, R. Multiple emitter location and signal parameter estimation. *IEEE Trans. Antennas Propag.* **1986**, *34*, 276–280. [[CrossRef](#)]
19. Roy, R.; Paulraj, A.; Kailath, T. ESPRIT—A subspace rotation approach to estimation of parameters of cisoids in noise. *IEEE Trans. Acoust. Speech Signal Process.* **1986**, *34*, 1340–1342. [[CrossRef](#)]
20. Kailath, T. ESPRIT—Estimation of signal parameters via rotational invariance techniques. *Opt. Eng.* **1990**, *29*, 296. [[CrossRef](#)]
21. Cardoso, J.-F.; Moulines, E. Asymptotic performance analysis of direction-finding algorithms based on fourth-order cumulants. *IEEE Trans. Signal Process.* **1995**, *43*, 214–224. [[CrossRef](#)]
22. Nikias, L.C.; Mendel, M.J. Signal processing with higher-order spectra. *Signal Process. Mag. IEEE* **1993**, *10*, 10–37. [[CrossRef](#)]
23. Abramovich, Y.I.; Gray, D.A.; Gorokhov, A.Y.; Spencer, N.K. Comparison of DoA estimation performance for various types of sparse antenna array geometries. In Proceedings of the 8th European Signal Processing Conference (EUSIPCO 1996), Trieste, Italy, 10–13 September 1996.
24. Vertatschitsch, E.; Haykin, S. Nonredundant arrays. *Proc. IEEE* **1986**, *74*, 217. [[CrossRef](#)]
25. Vaidyanathan, P.P.; Pal, P. Sparse sensing with co-prime samplers and arrays. *IEEE Trans. Signal Process.* **2011**, *59*, 573–586. [[CrossRef](#)]
26. Pal, P.; Vaidyanathan, P.P. Multiple level nested array: An efficient geometry for 2qth order cumulant based array processing. *IEEE Trans. Signal Process.* **2012**, *60*, 1253–1269. [[CrossRef](#)]
27. Iizuka, Y.; Ichige, K. Optimum linear array geometry with minimum redundancy for 2q-th order cumulant-based array processing. In Proceedings of the International Workshop on Compressed Sensing Theory and Its Applications to Radar, Aachen, Germany, 19–22 September 2016.
28. Mendel, M.J. Tutorial on higher-order statistics (spectra) in signal processing and system theory: Theoretical results and some applications. *IEEE Proc.* **1991**, *79*, 278–305. [[CrossRef](#)]
29. Moffet, A. Minimum-redundancy linear arrays. *IEEE Trans. Antennas Propag.* **1968**, *16*, 172–175. [[CrossRef](#)]
30. Pal, P.; Vaidyanathan, P.P. Nested arrays: A novel approach to array processing with enhanced degrees of freedom. *IEEE Trans. Signal Process.* **2010**, *58*, 4167–4181. [[CrossRef](#)]
31. Pillai, S.U.; Kwon, B.H. Forward/backward spatial smoothing techniques for coherent signal identification. *IEEE Trans. Acoust. Speech Signal Process.* **1989**, *37*, 8–15. [[CrossRef](#)]
32. Peng, Z.; Ding, Y.; Ren, S.; Wu, H.; Wang, W. Coprime nested arrays for DoA estimation: Exploiting the nesting property of coprime array. *IEEE Signal Process. Lett.* **2022**, *29*, 444–448. [[CrossRef](#)]
33. Liu, J.; Zhang, Y.; Lu, Y.; Ren, S.; Cao, S. Augmented nested arrays with enhanced DoF and reduced mutual coupling. *IEEE Trans. Signal Process.* **2017**, *65*, 5549–5563. [[CrossRef](#)]
34. Yang, M.; Sun, L.; Yuan, X.; Chen, B. Improved nested array with hole-free DCA and more degrees of freedom. *Electron. Lett.* **2016**, *52*, 2068–2070. [[CrossRef](#)]
35. Zheng, Z.; Wang, W.-Q.; Kong, Y.; Zhang, Y.D. Misc array: A new sparse array design achieving increased degrees of freedom and reduced mutual coupling effect. *IEEE Trans. Signal Process.* **2019**, *67*, 1728–1741. [[CrossRef](#)]

36. Ren, S.; Dong, W.; Li, X.; Wang, W.; Li, X. Extended nested arrays for consecutive virtual aperture enhancement. *IEEE Signal Process.* **2020**, *27*, 575–579. [[CrossRef](#)]
37. Liu, C.-L.; Vaidyanathan, P.P. Remarks on the spatial smoothing step in coarray music. *IEEE Signal Process. Lett.* **2015**, *22*, 1438–1442. [[CrossRef](#)]
38. Stoica, P.; Nehorai, A. Music, maximum likelihood and cramer-rao bound: Further results and comparisons. *IEEE Trans. Acoust. Speech Signal Process.* **1989**, *38*, 2605–2608.